Heliyon 10 (2024) e35528

Contents lists available at ScienceDirect

Heliyon

journal homepage: www.cell.com/heliyon

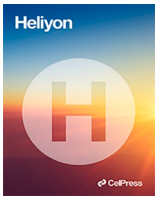

Research article

Dual-energy computed tomography for predicting cervical lymph node metastasis in laryngeal squamous cell carcinoma

Jianfei Tu [a,b,1], Guihan Lin [b,1], Weiyue Chen [b,1], Feng Cheng [c], Haifeng Ying [b], Chunli Kong [b], Dengke Zhang [b], Yi Zhong [b], Yongjun Ye [b], Minjiang Chen [b], Chenying Lu [b], Xiaomin Yue [a], Wei Yang [a,*]

[a] *Department of Biophysics and Department of Neurosurgery, The Fourth Affiliated Hospital, Zhejiang University School of Medicine, Hangzhou, Zhejiang, 310058, China*

[b] *Key Laboratory of Imaging Diagnosis and Minimally Invasive Intervention Research, Zhejiang Engineering Research Center of Interventional Medicine Engineering and Biotechnology, Key Laboratory of Precision Medicine of Lishui City, The Fifth Affiliated Hospital of Wenzhou Medical University, Lishui 323000, China*

[c] *Department of Head and Neck Surgery, The Fifth Affiliated Hospital of Wenzhou Medical University, Lishui, 323000, China*

ARTICLE INFO

Keywords:
Dual-energy computed tomography
Laryngeal squamous cell carcinoma
Lymph node metastasis
Prediction model
Nomogram

ABSTRACT

Rationale and objectives: We constructed a dual-energy computed tomography (DECT)-based model to assess cervical lymph node metastasis (LNM) in patients with laryngeal squamous cell carcinoma (LSCC).

Materials and methods: We retrospectively analysed 164 patients with LSCC who underwent preoperative DECT from May 2019 to May 2023. The patients were randomly divided into training (n = 115) and validation (n = 49) cohorts. Quantitative DECT parameters of the primary tumours and their clinical characteristics were collected. A logistic regression model was used to determine independent predictors of LNM, and a nomogram was constructed along with a corresponding online model. Model performance was assessed using the area under the curve (AUC) and the calibration curve, and the clinical value was evaluated using decision curve analysis (DCA).

Results: In total, 64/164 (39.0 %) patients with LSCC had cervical LNM. Independent predictors of LNM included normalized iodine concentration in the arterial phase (odds ratio [OR]: 8.332, 95 % confidence interval [CI]: 2.813–24.678, $P < 0.001$), normalized effective atomic number in the arterial phase (OR: 5.518, 95 % CI: 1.095–27.818, $P = 0.002$), clinical T3-4 stage (OR: 5.684, 95 % CI: 1.701–18.989, $P = 0.005$), and poor histological grade (OR: 5.011, 95 % CI: 1.003–25.026, $P = 0.049$). These predictors were incorporated into the DECT-based nomogram and the corresponding online model, showing good calibration and favourable performance (training AUC: 0.910, validation AUC: 0.918). The DCA indicated a significant clinical benefit of the nomogram for estimating LNM.

Conclusions: DECT parameters may be useful independent predictors of LNM in patients with LSCC, and a DECT-based nomogram may be helpful in clinical decision-making.

* Corresponding author. Department of Biophysics, Department of Neurology of the Fourth Affiliated Hospital, Zhejiang University School of Medicine, Hangzhou, 310000, China.

E-mail address: yangwei@zju.edu.cn (W. Yang).

[1] Jianfei Tu, Guihan Lin and Weiyue Chen contributed equally to this work.

https://doi.org/10.1016/j.heliyon.2024.e35528
Received 18 March 2024; Received in revised form 22 July 2024; Accepted 30 July 2024
Available online 31 July 2024

Abbreviations

AUC	area under the receive operating characteristic curve
AP	arterial phase
CI	confidence interval
DCA	decision curve analysis
DECT	dual-energy computed tomography
ICC	interclass correlation coefficients
IC	iodine concentration
LNM	lymph node metastasis
LSCC	laryngeal squamous cell carcinoma
MRI	magnetic resonance imaging
NIC	normalized iodine concentration
nZ_{eff}	normalized effective atomic number
OR	odds ratio
PET/CT	positron emission tomography/computed tomography
ROC	receiver operating characteristic
ROI	region of interest
λ_{HU}	slope of the spectral Hounsfield unit curve
VP	venous phase
Z_{eff}	effective atomic number

1. Introduction

Laryngeal squamous cell carcinoma (LSCC) is one of the most common malignancies of the head and neck, and the morbidity and mortality rates associated with this cancer are increasing annually [1]. In 2020, 180,000 new cases of LSCC and almost 100,000 LSCC-related deaths were reported globally [2]. The current comprehensive treatment for LSCC depends primarily on surgical intervention and radiotherapy. However, despite recent improvements in techniques and the emergence of new anticancer medications, a significant number of patients still have poor prognosis and short survival times, notably those with cervical lymph node metastasis (LNM) [3,4]. The effect of LNM on the curability of LSCC is more significant than that of the primary lesions. LNM failure is the most likely cause of treatment failure [5–7]. Therefore, the accurate preoperative identification of cervical LNM in patients with LSCC is essential for selecting an optimal treatment plan that can improve prognosis.

Currently, imaging methods such as ultrasonography, magnetic resonance imaging (MRI), positron emission tomography/computed tomography (PET/CT), and CT are widely used to evaluate LNM before treatment initiation [8]. Ultrasound is economical and convenient; however, the thyroid cartilage limits the accurate determination of LNM in the posterior laryngeal cavity, and image quality is influenced by the operator's skill. MRI has good contrast for soft tissues but has a low spatial resolution, long scan time, and artefacts that can appear due to swallowing and respiratory movement. PET-CT combines anatomical and functional metabolic information and facilitates the accurate diagnosis of lesions. However, studies have shown that it has low sensitivity for cervical LNM diagnosis in LSCC [9]. Because of its high efficiency and large imaging range, CT is the most widely used imaging method for evaluating LSCC before treatment initiation. However, identifying cervical LNM based on morphology is very challenging, with a previously reported diagnostic accuracy of only 60–80 % [10,11].

Dual-energy CT (DECT) technology can reconstruct various spectral images, including virtual monoenergetic, iodine concentration (IC), effective atomic number (Z_{eff}), and virtual non-contrast (VNC) images, without increasing the radiation dose [12,13]. Compared to conventional CT, DECT provides more comprehensive information for the differential diagnosis of tumours [14]. In addition to assessing the morphological characteristics, DECT can be used to quantitatively analyse lesions. In recent years, DECT has shown potential for preoperative assessment of LNM in oral [15], thyroid [16], breast [17], and colorectal [18] cancers. However, only a few studies have predicted LNM in patients with LSCC [19]. In this study, we evaluated a DECT-based nomogram that combined multiple DECT parameters of the primary tumour with clinical risk factors to predict cervical LNM before surgery in patients with LSCC.

2. Materials and methods

2.1. Patient selection

This study was approved by the Institutional Review Board and the Human Ethics Committee of XXXX (No. 2023-508). The requirement for informed consent was waived because of the retrospective nature of the study. From May 2019 to May 2023, 405 consecutive patients with LSCC who underwent DECT were selected from XXXX. Patients were enrolled if they met the following inclusion criteria [1]: confirmed LSCC diagnosed by surgery or biopsy [2], curative open surgery and lymphadenectomy performed with complete pathology results, and [3] DECT performed within 2 weeks before surgery with satisfactory image quality. The exclusion criteria were as follows [1]: prior history of surgical or radiotherapy treatment of the neck [2]; presence of distant metastases

before surgery [3]; concomitant head and neck tumours at other sites, such as thyroid cancer [4]; LSCC lesions not identified on DECT-derived images; and [5] incomplete clinical data and demographic information. A total of 164 patients met the inclusion criteria and were included in this study. They were randomly divided into training (n = 115) and validation (n = 49) cohorts at a ratio of 3:1. The patient screening pathway is shown in Fig. 1.

2.2. Surgical procedure

All patients underwent partial or total laryngectomy according to the extent of the primary tumour, as determined by preoperative examination, as recommended by the National Comprehensive Cancer Network guidelines [20]. All patients underwent elective neck dissection. Bilateral neck sweeps were performed when the tumour approached or crossed the sagittal midline. Unilateral neck dissection was performed for the unilateral primary tumours. Patients who underwent unilateral dissection were closely followed. All dissected lymph nodes (LNs) were examined using haematoxylin-eosin staining. According to the postoperative pathology results, all patients in our study were classified as either LNM (+) or LNM (−).

2.3. Image acquisition and postprocessing

A third-generation 192-slice DECT scanner (Somatom Force; Siemens Medical Solutions) was used for plain and enhanced neck scans. To reduce motion artefacts, the patients were instructed to avoid swallowing during the scan. All patients were scanned in the supine position, with their hands above their heads. Scanning was performed from the base of the skull to the thoracic entrance level. After a flat scan, enhanced scanning was performed in the dual-energy mode with a current of 50 mA and a voltage of Sn 140-kVp for Tube A, and a current of 100-mA and voltage of 80-kVp for Tube B. The tube current was adjusted with the CARE Dose 4D enabled, with 1.0 pitch, 0.5 s/r rack speed, 192 × 0.6 mm collimator width, and a high and low tube voltage fusion factor of 0.5. A model-based iterative reconstruction algorithm was used to improve the image quality. Reconstruction was performed using a convolution kernel (Qr40, Siemens) with a slice thickness of 1.0 mm and an interval of 1.0 mm. The contrast agent iopromide (370 mg/mL, Shering) was injected through the elbow vein at a flow rate of 3.0 mL/s using a double-tube high-pressure syringe (total dose 1.0 mL/kg), followed by 30 mL of saline. Arterial and venous phase scanning was performed 30 s and 70 s after injection of the contrast medium [18].

2.4. Image analysis

All the data were transmitted to a post-processing workstation (Syngo VA10B, Siemens Healthcare) for analysis. DECT parameters were independently measured by two radiologists (Y.H.F. and Y.Y.J., with 12 and 15 years of head and neck imaging experience, respectively), both of whom were blinded to the patients' clinical history and pathology. The IC and Z_{eff} of the tumour were measured in 'Live VNC' and 'Rho/Z' modes, respectively, and placed the region of interest (ROI) at the same level as the internal carotid artery. To reduce differences between patients, the normalized iodine concentration (NIC) and normalized effective atomic number (nZ_{eff}) were calculated using the following formulas:

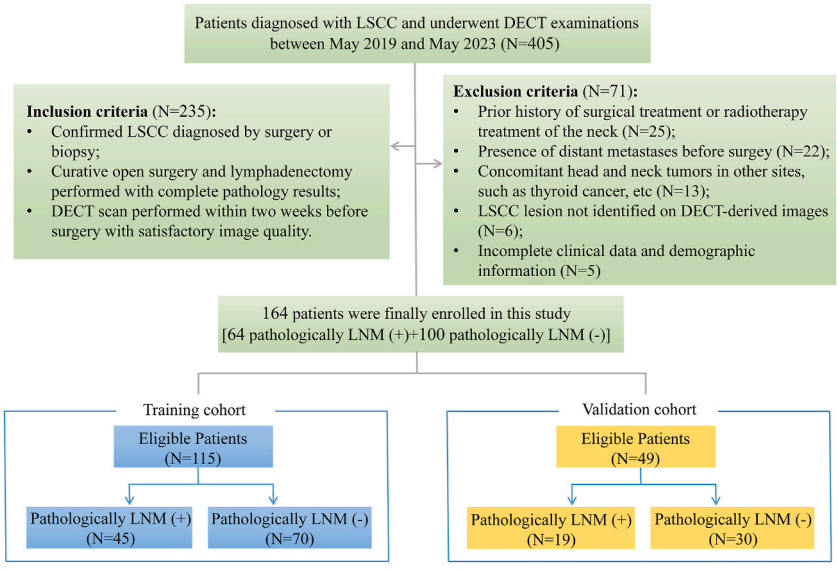

Fig. 1. Patient screening procedure. DECT, dual-energy computed tomography; LNM, lymph node metastasis; LSCC, laryngeal squamous cell carcinoma.

$$NIC = \frac{IC_{tumor}}{IC_{artery}}\ ;\ nZ_{eff} = \frac{Zeff_{tumor}}{Zeff_{artery}}$$

The energy spectrum attenuation curve of the tumour was obtained using 'Monoenergetic Plus' mode, and the slope of the spectral curve (λ_{HU}) was calculated using the following formula:

$$\lambda_{HU} = \frac{(CT_{40\ kev} - CT_{70\ kev})}{30}$$

To ensure the accuracy of the ROI measurement, the following standards were set [1]: the ROI was measured at the maximum cross-section of the visible tumour, and calcification, necrosis, blood vessels, and lesion edges were avoided as much as possible [2]; the ROI within the tumour was controlled within approximately 70–80 % of the total area of the largest slice [3]; the size, shape, and position of the ROI were consistent during different modes and phases of measurement; and [4] all images were measured three times and averaged.

2.5. Clinical and pathological information

Demographic information and clinical histories were retrospectively collected from the patients' medical records. These included

Table 1
Comparison of clinical and conventional CT characteristics in pathological LNM (+) and LNM (−) patients with laryngeal squamous cell carcinoma in the training cohort.

Characteristic	Training cohort (n = 115)		*P* value	Validation cohort (n = 49)		*P* value
	Pathologically LNM (+) (n = 45)	Pathologically LNM (−) (n = 70)		Pathologically LNM (+) (n = 19)	Pathologically LNM (−) (n = 30)	
Age (years)			0.595			0.761
<65	24 (53.3)	43 (61.4)		12 (63.2)	18 (60.0)	
≥65	21 (46.7)	27 (38.6)		7 (36.8)	12 (40.0)	
Sex			0.734			0.739
Female	4 (8.9)	5 (7.1)		1 (5.3)	1 (3.3)	
Male	41 (91.1)	65 (92.9)		18 (94.7)	29 (96.7)	
Cigarette smoking			0.683			0.515
No	7 (15.6)	9 (12.9)		0 (0.0)	2 (6.7)	
Yes	38 (84.4)	61 (87.1)		19 (100.0)	28 (93.3)	
Alcohol drinking			0.724			0.729
No	14 (31.1)	24 (34.3)		5 (26.3)	6 (20.0)	
Yes	31 (68.9)	46 (65.7)		14 (73.7)	24 (80.0)	
Histological grade			**0.003**			**0.028**
Well	8 (17.8)	19 (27.1)		2 (10.5)	7 (23.3)	
Moderate	15 (33.3)	38 (54.3)		7 (36.8)	18 (70.0)	
Poor	22 (48.9)	13 (18.6)		10 (52.7)	5 (16.7)	
Tumour size	2.57 ± 0.73	2.38 ± 0.54	0.146	2.45 ± 0.61	2.35 ± 0.48	0.543
Tumour location			**0.019**			**0.023**
Supraglottic	26 (57.8)	22 (31.4)		11 (57.8)	8 (26.6)	
Glottic	17 (37.8)	44 (62.9)		7 (36.8)	22 (73.4)	
Subglottic	2 (4.4)	4 (5.7)		1 (5.4)	0 (0.0)	
Clinical T stage			< **0.001**			**0.014**
T1-2	14 (31.1)	48 (68.6)		8 (42.1)	23 (76.7)	
T3-4	31 (68.9)	22 (31.4)		11 (57.9)	7 (23.3)	
Tumour depth			**0.029**			**0.018**
Muscular layer	21 (46.7)	47 (67.1)		9 (47.3)	24 (80.0)	
Mucosa or submucosa	24 (53.3)	23 (32.9)		10 (52.7)	6 (20.0)	
Resection margin			0.321			0.635
Negative	4 (8.9)	3 (4.3)		2 (10.5)	2 (6.7)	
Positive	41 (91.1)	67 (95.7)		17 (89.5)	28 (93.3)	
Thyroid cartilage invasion			**0.016**			**0.030**
Absent	16 (35.6)	41 (58.6)		6 (31.6)	19 (63.3)	
Present	29 (64.4)	29 (41.4)		13 (68.4)	11 (36.7)	
Pre-epiglottic space involvement			0.197			0.362
Absent	32 (71.1)	57 (81.4)		13 (68.4)	24 (80.0)	
Present	13 (28.9)	13 (18.6)		6 (31.6)	6 (20.0)	
CT-reported LNM status			0.118			0.221
Negative	19 (42.2)	40 (57.1)		8 (42.1)	18 (60.0)	
Positive	26 (57.8)	30 (42.9)		11 (57.9)	12 (40.0)	

Abbreviations: CT, computed tomography; LNM, lymph node metastasis.

age, sex, cigarette smoking, alcohol consumption, tumour size, location, histological grade, clinical T stage, depth, resection margin, thyroid cartilage invasion, pre-epiglottic space involvement, and CT-reported LNM status. Patients were divided into two groups according to age (<65 and ≥65 years) [21]. The histological grade was based on the biopsy results, and cancer was staged according to the eighth edition of the 2017 International Union Against Cancer [22]. The lymphadenectomy site for each patient was based on a comprehensive assessment of tumour size, location, and important clinical or imaging findings, in line with the American Society of Clinical Oncology clinical practice guidelines [23]. A positive CT report for LNM should meet at least one of the following criteria [1]: a short diameter of ≥10 mm [2]; marked enhancement similar to that of the pharyngeal mucosa [3]; uneven enhancement [4]; cystic degeneration, necrosis, or calcification; and [5] extranodal extension, poorly defined borders, or invasion of adjacent tissues.

2.6. Statistical analysis

Statistical analyses were performed using SPSS (version 26.0) and R software (version 4.1.0). Categorical variables were expressed as numbers (proportion, %) and compared using χ^2 or Fisher's exact tests. Continuous variables were expressed as mean ± standard deviation or median (interquartile range) and compared using Student's t-test or Mann–Whitney *U* test. The intraclass correlation coefficient (ICC) with a 95 % confidence interval (CI) was used to evaluate the inter-reader reproducibility of the DECT-derived parameters. An ICC >0.75 was considered to indicate good agreement. Univariate and multivariate logistic regression analyses were performed to identify independent predictors of LNM. Significant variables ($P < 0.10$) in the univariate analyses of the training cohort were included in multivariate analysis using forward stepwise variable selection. Tolerance and variance inflation factors (VIFs) were used to evaluate the multicollinearity in the multivariate model. Based on the results of the multivariate analysis, a prediction model and corresponding nomogram were constructed to predict LNM in patients with LSCC in the training cohort and were then tested in the validation cohort. Additionally, an internet browser model based on the nomogram was programmed using the 'DynNom' package in R software. To assess the nomogram fit, the predictive performance was evaluated through discrimination and calibration. Model discrimination was assessed using receiver operating characteristic (ROC) curves, and the areas under the ROC curves (AUCs), sensitivity, specificity, and accuracy were calculated. The DeLong test was used to compare the differences in AUC between the DECT-based nomogram, the DECT model, and the clinical model. Model calibration was evaluated using the Hosmer–Lemeshow test with 1000 bootstrap samples and its visualised calibration curves. Decision curve analysis (DCA) was performed to verify the clinical value of the model by estimating the net benefit to patients under different threshold probabilities. Statistical significance was defined as a two-tailed *P* value < 0.05.

3. Results

3.1. Clinical and conventional CT characteristics

The baseline patient characteristics are presented in Table 1. The number of patients in the two cohorts was similar at baseline (Table S1). According to the pathology results, 45 (39.1 %) patients in the training cohort were LNM (+) and 70 (60.9 %) were LNM (−), while in the validation cohort, 19 (38.8 %) were LNM (+) and 30 (61.2 %) were LNM (−). In the entire cohort, there were 79 clinically LN-positive and 85 clinically LN-negative patients based on CT evaluation. Among them, 42.2 % (27/64) of pathological LNM (+) patients were understaged as CT-reported LNM (−), and 42.0 % (42/100) of pathological LNM (−) patients were overstaged as CT-reported LNM (+). There was no significant difference between the two cohorts ($P = 0.966$). The histological grade and

Table 2
Comparison of dual-energy CT parameters in pathological LNM (+) and LNM (−) patients with laryngeal squamous cell carcinoma and the performance of each parameter for predicting LNM.

Parameter	Pathologically LNM (+) (N = 64)	Pathologically LNM (−) (N = 100)	*P* value	AUC (95 % CI)	Sensitivity (%)	Specificity (%)	Accuracy (%)
NIC							
In the arterial phase	0.30 (0.24–0.40)	0.22 (0.17–0.27)	<0.001	0.804 (0.735–0.862)	92.2 (88.1–96.3)	52.0 (44.4–59.6)	67.7 (60.5–74.9)
In the venous phase	0.52 (0.38–0.64)	0.45 (0.35–0.53)	<0.001	0.663 (0.585–0.735)	35.9 (28.6–43.2)	93.0 (89.1–96.9)	70.7 (63.7–77.7)
λ_{HU} (HU/keV)							
In the arterial phase	4.68 (3.92–5.70)	4.03 (3.42–5.19)	0.020	0.608 (0.529–0.683)	48.4 (40.8–56.1)	71.0 (64.1–77.9)	62.2 (54.8–69.6)
In the venous phase	4.22 (3.11–5.00)	3.79 (3.08–4.30)	0.089	0.579 (0.499–0.655)	48.4 (40.8–56.1)	81.0 (75.0–87.0)	68.3 (61.2–75.4)
nZ_{eff}							
In the arterial phase	0.78 (0.75–0.82)	0.73 (0.71–0.76)	<0.001	0.756 (0.682–0.819)	78.1 (71.8–84.4)	62.0 (54.6–69.4)	68.3 (61.2–75.4)
In the venous phase	0.91 (0.86–0.93)	0.88 (0.85–0.91)	0.087	0.610 (0.531–0.686)	54.7 (47.1–62.3)	71.0 (64.1–77.9)	64.6 (57.3–71.9)

Abbreviations: AUC, area under the curve; CT, computed tomography; CI, confidence interval; LNM, lymph node metastasis; NIC, normalized iodine concentration; λ_{HU}, slope of the spectral Hounsfield unit curve; nZ_{eff}, normalized effective atomic number.

conventional CT characteristics of the primary lesion, including tumour location, clinical T stage, tumour depth, and the presence of thyroid cartilage invasion, were significantly correlated with LNM (+) pathology in the training and validation cohorts (all $P < 0.05$). However, other demographic and clinical variables such as age, sex, history of cigarette smoking and alcohol consumption, tumour size, resection margin, and pre-epiglottic space involvement were not significantly associated with LNM (+) pathology in either cohort (all $P > 0.05$).

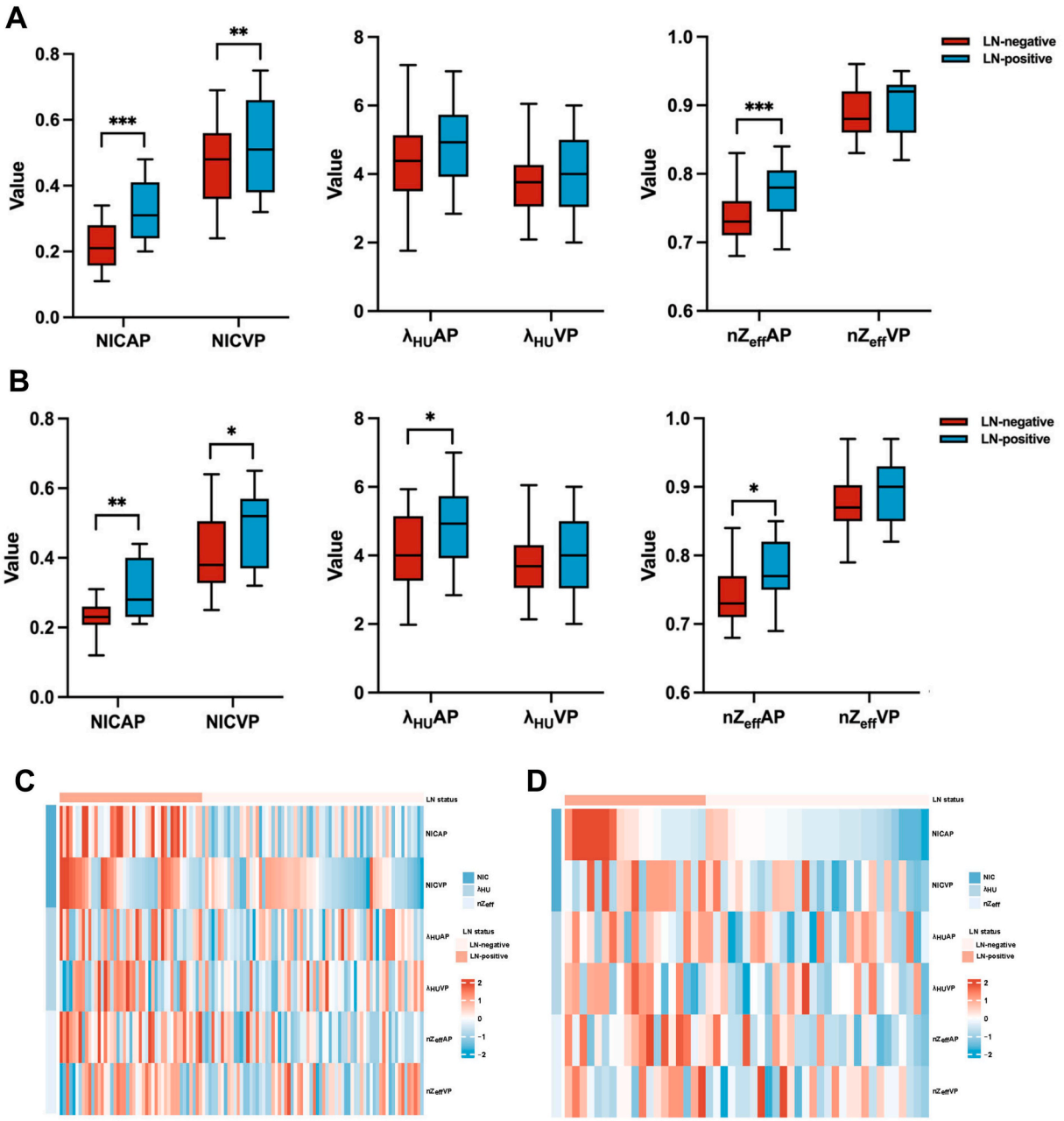

Fig. 2. Box plots showing NIC, $\lambda_{HU,}$ and nZ_{eff} in the training (**A**) and validation (**B**) cohorts. Heatmaps showing the correlation between DECT quantitative parameters and LN pathology in the training (**C**) and validation (**D**) cohorts. DECT, dual-energy computed tomography; LN, lymph node; NICAP, normalized iodine concentration in arterial phase; NICVP, normalized iodine concentration in venous phase; $nZ_{eff}AP$, normalized effective atomic number in the arterial phase; $nZ_{eff}VP$, normalized effective atomic number in the venous phase; $\lambda_{HU}AP$, slope of the spectral Hounsfield unit curve in the arterial phase; $\lambda_{HU}VP$, slope of the spectral Hounsfield unit curve in the venous phase. $^{*}P < 0.05$, $^{**}P < 0.01$, $^{***}P < 0.001$.

3.2. DECT quantitative parameters

Quantitative DECT parameters were obtained from primary tumours. As shown in Table S2, excellent inter-reader agreement was observed for the measurement of DECT parameters, with ICC values ranging from 0.908 to 0.962. NIC in the arterial phase (NICAP) and in the venous phase (NICVP), nZ_{eff} in the arterial phase (nZ_{eff}AP), and λ_{HU} in the arterial phase (λ_{HU}AP) were slightly higher in patients with LNM (+) pathology than in those who were LNM (−) in the entire cohort (all $P < 0.05$) (Table 2). In addition, patients who were LNM (+) had significantly higher NICAP, NICVP, and nZ_{eff}AP than those who were LNM (−) in both the training and validation cohorts (all $P < 0.05$) (Fig. 2A, B and Table S3). Correlation analyses of DECT quantitative parameters and LNM status are shown in Fig. 2C and D, and Table S4. ROC curve analysis showed that AUC values for NICAP, NICVP, nZ_{eff}AP, nZ_{eff} in the venous phase (nZ_{eff}VP), λ_{HU}AP, and λ_{HU} in the venous phase (λ_{HU}VP) that could allow differentiation between patients who were LNM (+) and LNM (−) were 0.804, 0.663, 0.756, 0.610, 0.608, and 0.579, respectively. The detailed results are presented in Table 2.

3.3. Predictors of LNM (+) pathology and development of the prediction model

All significant variables ($P < 0.1$) found in the univariate logistic regression analyses of the training cohort were included in the multivariate analysis (Table S5). The VIF for each variable in the prediction model was <10, and the tolerance was >0.1 (Table S6). Multivariate analyses showed that the clinical T3-4 stage (OR: 5.684, 95 % CI: 1.701–18.989, $P = 0.005$), poor histological grade (OR: 5.011, 95 % CI: 1.003–25.026, $P = 0.049$), NICAP (OR: 8.332, 95 % CI: 2.813–24.678, $P < 0.001$), and nZ_{eff}AP (OR: 5.518, 95 % CI: 1.095–27.818, $P = 0.002$) were independent predictors of LNM (+) status in patients with LSCC (Fig. 3). A DECT-based nomogram model that included these four independent predictors was constructed, as shown in Fig. 4A. Each variable is assigned a score on a point scale. The probability of LNM (+) status was determined by adding the scores of each variable to obtain a total and then drawing a vertical line. As shown in Fig. 4B, a free browser-based version of the model was developed, which can be accessed at https://lnmpredictmodel.shinyapps.io/LNM_Prediction_Nomogram/. In parallel, the clinical and DECT models were constructed using multivariate regression analyses, as shown in Fig. S1.

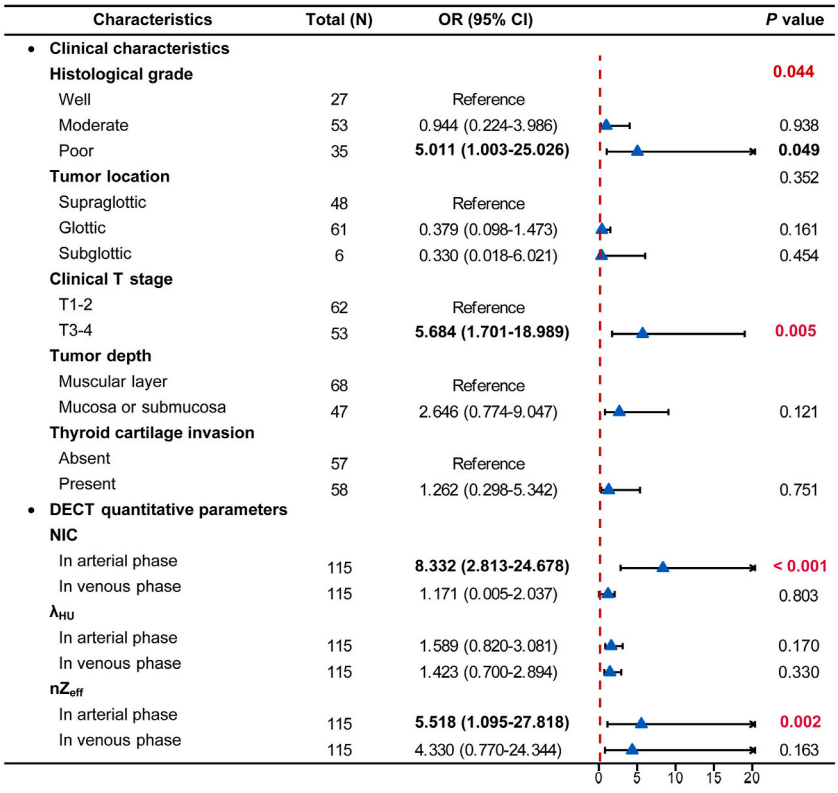

Fig. 3. Forest plot showing multivariate analysis of independent predictors of LNM (+) pathology in patients with LSCC in the training cohort. A logistic regression model was used to estimate ORs and 95 % CIs. CI, confidence interval; DECT, dual-energy computed tomography; LNM, lymph node metastases; LSCC, laryngeal squamous cell carcinoma; NIC, normalized iodine concentration; λ_{HU}, slope of the spectral Hounsfield unit curve; nZ_{eff}, normalized effective atomic number; OR, odds ratio.

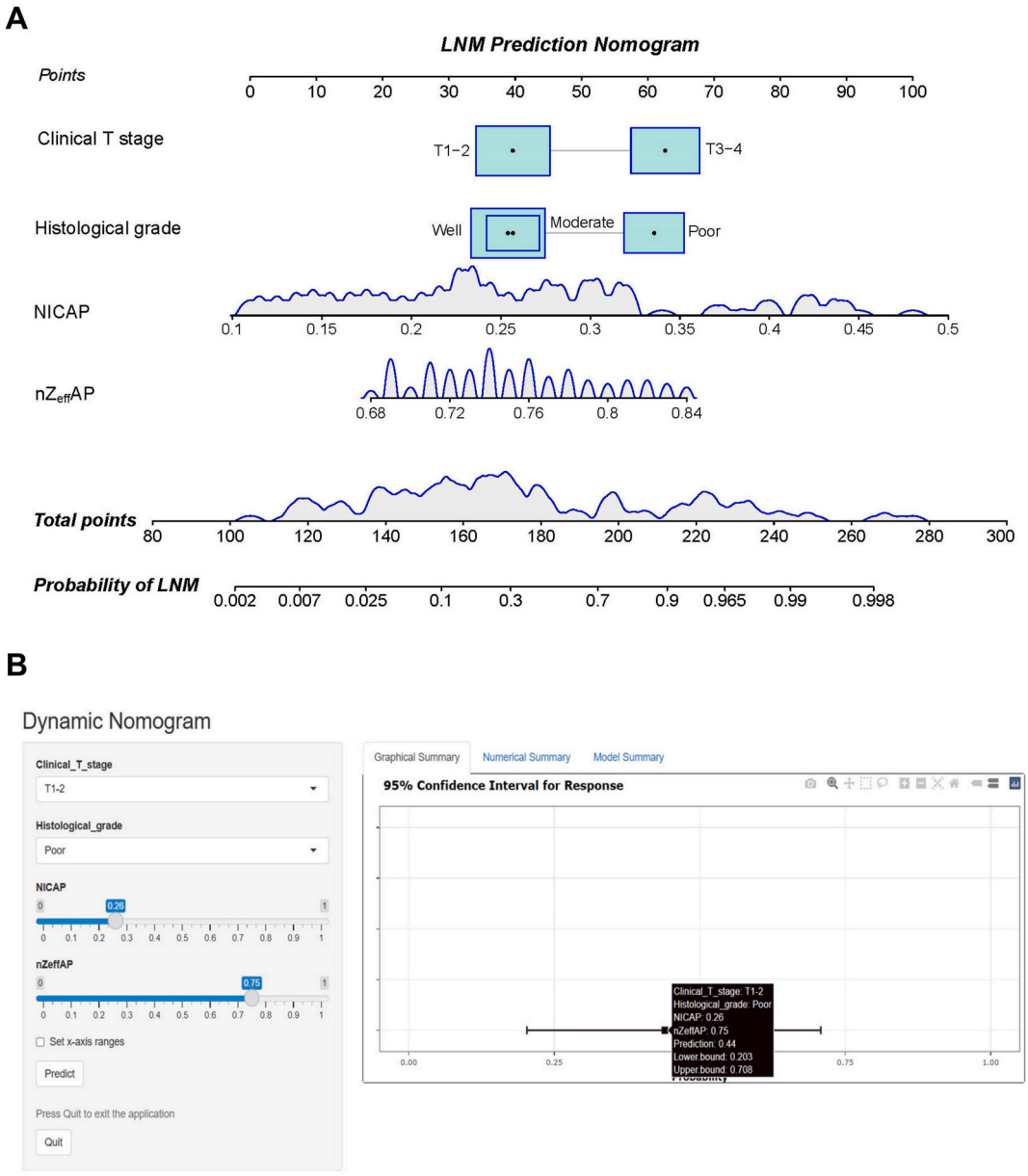

Fig. 4. Nomogram model (**A**) and online free browser-based model (**B**) for predicting the probability of LNM (+) pathology in LSCC patients. LNM, lymph node metastases; LSCC, laryngeal squamous cell carcinoma; NICAP, normalized iodine concentration in the arterial phase; $nZ_{eff}AP$, normalized effective atomic number in the arterial phase.

3.4. Performance evaluation and clinical applicability

The DECT-based nomogram had good performance for predicting the probability of LNM, with AUCs of 0.910 (95 % CI: 0.850–0.969) in the training cohort and 0.918 (95 % CI: 0.803–0.977) in the validation cohort (Fig. 5A and B, Table 3). The diagnostic efficacy of the nomogram was significantly better than that of the clinical model based on the clinical T stage and histological grade in both the training ($Z = 3.160$, $P = 0.002$) and validation cohorts ($Z = 2.212$, $P = 0.027$) (Table 4). Although there were no significant differences in the AUCs between the nomogram and the DECT model based on NICAP and $nZ_{eff}AP$ in the two cohorts, the nomogram showed better sensitivity, specificity, and accuracy, with respective values of 82.2 %, 94.3 %, and 89.6 % in the training cohort, and 89.5 %, 83.3 %, and 85.7 % in the validation cohort (Table 3). The calibration plot of the nomogram had a good fit and showed good agreement between predictions and observations in both cohorts, with mean absolute errors of 0.025 and 0.020, respectively (Fig. 5C and D).

Based on the DCA, the DECT-based nomogram had the highest curve within the risk threshold range of 8–91 % in the training

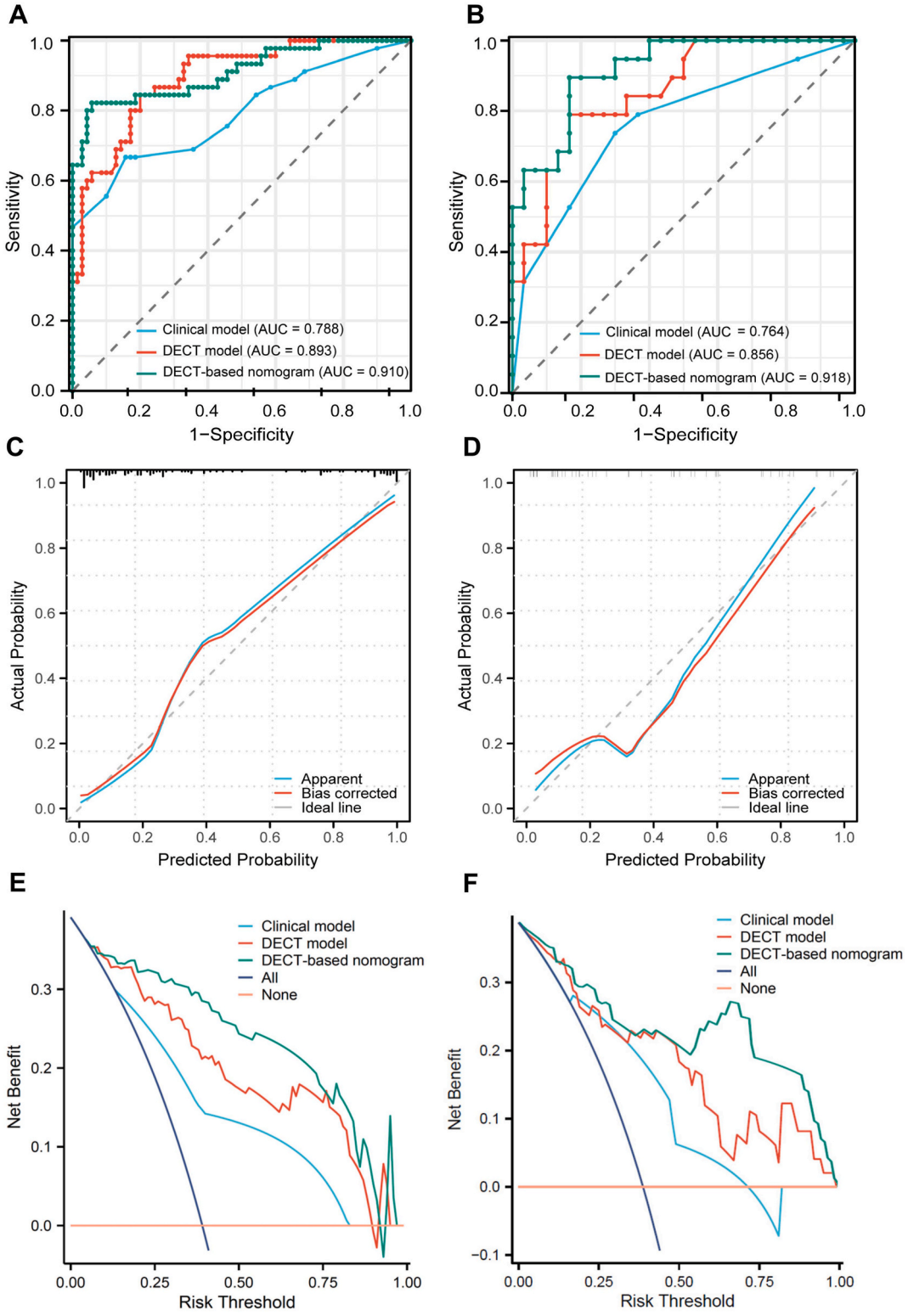

Fig. 5. ROC curves showing the performance of the clinical model, DECT model, and DECT-based nomogram for discriminating LNM (+) pathology in the training (**A**) and validation cohorts (**B**). Calibration curves of the DECT-based nomogram in the training (**C**) and validation cohorts (**D**). Decision curve of the clinical model, DECT model, and DECT-based nomogram in the training (**E**) and validation cohorts (**F**). AUC, area under the curve; DECT, dual-energy computed tomography; LNM, lymph node metastasis; ROC, receiver operating characteristic.

Table 3
Performance of three proposed models (clinical model, DECT model, and DECT-based nomogram) for predicting pathological LNM (+) of laryngeal squamous cell carcinoma in the training and validation cohorts.

Models	Cohorts	AUC (95 % CI)	Sensitivity (%)	Specificity (%)	Accuracy (%)
Clinical model	Training	0.788 (0.698–0.879)	66.7 (51.0–80.0)	84.3 (73.6–91.9)	77.4 (69.8–85.0)
	Validation	0.764 (0.624–0.904)	73.7 (48.8–90.9)	70.0 (50.6–85.3)	71.4 (58.7–84.1)
DECT model	Training	0.893 (0.835–0.950)	84.4 (70.5–93.5)	80.0 (68.7–88.6)	81.7 (74.6–88.8)
	Validation	0.856 (0.726–0.940)	78.9 (54.4–93.9)	83.3 (65.3–94.4)	83.6 (73.2–94.0)
DECT-based nomogram	Training	0.910 (0.850–0.969)	82.2 (67.9–92.0)	94.3 (86.0–98.4)	89.6 (84.0–95.2)
	Validation	0.918 (0.803–0.977)	89.5 (66.9–98.7)	83.3 (65.3–94.4)	85.7 (75.9–95.5)

Abbreviations: AUC, area under the curve; CI, confidence interval; DECT, dual-energy computed tomography; LNM, lymph node metastasis.

Table 4
Comparisons of AUCs between the clinical model, DECT model, and DECT-based nomogram in the training and validation cohorts.

Comparisons	AUC	
	Z*	*P* value
Training cohort		
DECT model *vs.* Clinical model	2.024	**0.043**
DECT-based nomogram *vs.* Clinical model	3.160	**0.002**
DECT-based nomogram *vs.* DECT model	0.742	0.458
Validation cohort		
DECT model *vs.* Clinical model	0.967	0.333
DECT-based nomogram *vs.* Clinical model	2.212	**0.027**
DECT-based nomogram *vs.* DECT model	1.669	0.095

Abbreviations: AUC, area under the curve; DECT, dual-energy CT.

cohort (Fig. 5E) and 19–100 % in the validation cohort (Fig. 5F), suggesting that the nomogram was more likely to predict LNM in patients with LSCC than the DECT or clinical models. In real-world clinical applications, users can enter information related to independent risk factors in a free browser-based model, and the probability of LNM is automatically generated and displayed. Two examples of the clinical application of this easy-to-use model are shown in Figs. 6 and 7.

3.5. Subgroup prediction performance of the nomogram

Subgroup analyses, separately stratified by tumour location, were conducted across the entire patient population. In the training cohort, the DECT-based nomogram yielded an AUC of 0.909 (95 % CI: 0.825–0.993) in the supraglottic group and 0.897 (95 % CI: 0.800–0.994) in the glottic-subglottic group. In the validation cohort, the DECT-based nomogram had an AUC of 0.875 (95 % CI: 0.708–1.000) in the supraglottic group and 0.926 (95 % CI: 0.809–1.000) in the glottic-subglottic group. The DeLong test showed no statistically significant differences among the subgroup analyses in the training ($Z = 0.186$, $P = 0.853$) and validation ($Z = 0.491$, $P = 0.626$) cohorts. The subgroup prediction performance and AUCs are presented in Table S7 and Fig. S2.

4. Discussion

To our knowledge, this is the first study to develop a DECT-based prediction model that combines DECT parameters and clinical factors to predict LNM in patients with LSCC. The combined model performed better and was more clinically useful than the models based solely on clinical or DECT findings. In addition, the free browser-based version of the model is an easy-to-use individualised tool for evaluating LNM status, which may help in clinical decision-making for personalised treatment.

The larynx has a high concentration of lymphoid tissue, making patients with LSCC highly vulnerable to cervical LNM. Once LNM develops, the tumour is classified as intermediate to advanced, and the 5-year survival rate is significantly reduced [3,24]. LNM has a greater impact on the cure rate of LSCC than primary lesions, with metastatic LNs being a major cause of treatment failure [25,26]. Therefore, the preoperative determination of LN status is critical to determine the need for neck dissection or other adjuvant treatments [7,23,27]. Several methods have been proposed to predict LNM in patients with LSCC, including clinical models, molecular markers, and sentinel LN biopsy [28–30]. However, their effectiveness and practicality have been unsatisfactory. In recent years, DECT has shown excellent capabilities for predicting the histopathological characteristics of head and neck cancers [31,32]. A previous study analysed 399 cervical LNs from 103 patients using DECT (15). Although the results showed impressive performance, this study primarily focused on analysing LN images, requiring a one-to-one correspondence with the pathology results. Previous studies have shown a correlation between DECT parameters of primary tumours and LNM [33,34]. Thus, we hypothesised that DECT image analysis of primary tumours could be a reasonable method for predicting LNM in LSCC.

Prior studies have reported that the risk of cervical LNM in patients with LSCC is associated with disease factors such as T stage, tumour location, and histological grade [35–38]. Our study suggests that the risk of LNM increases with higher clinical T stage, which

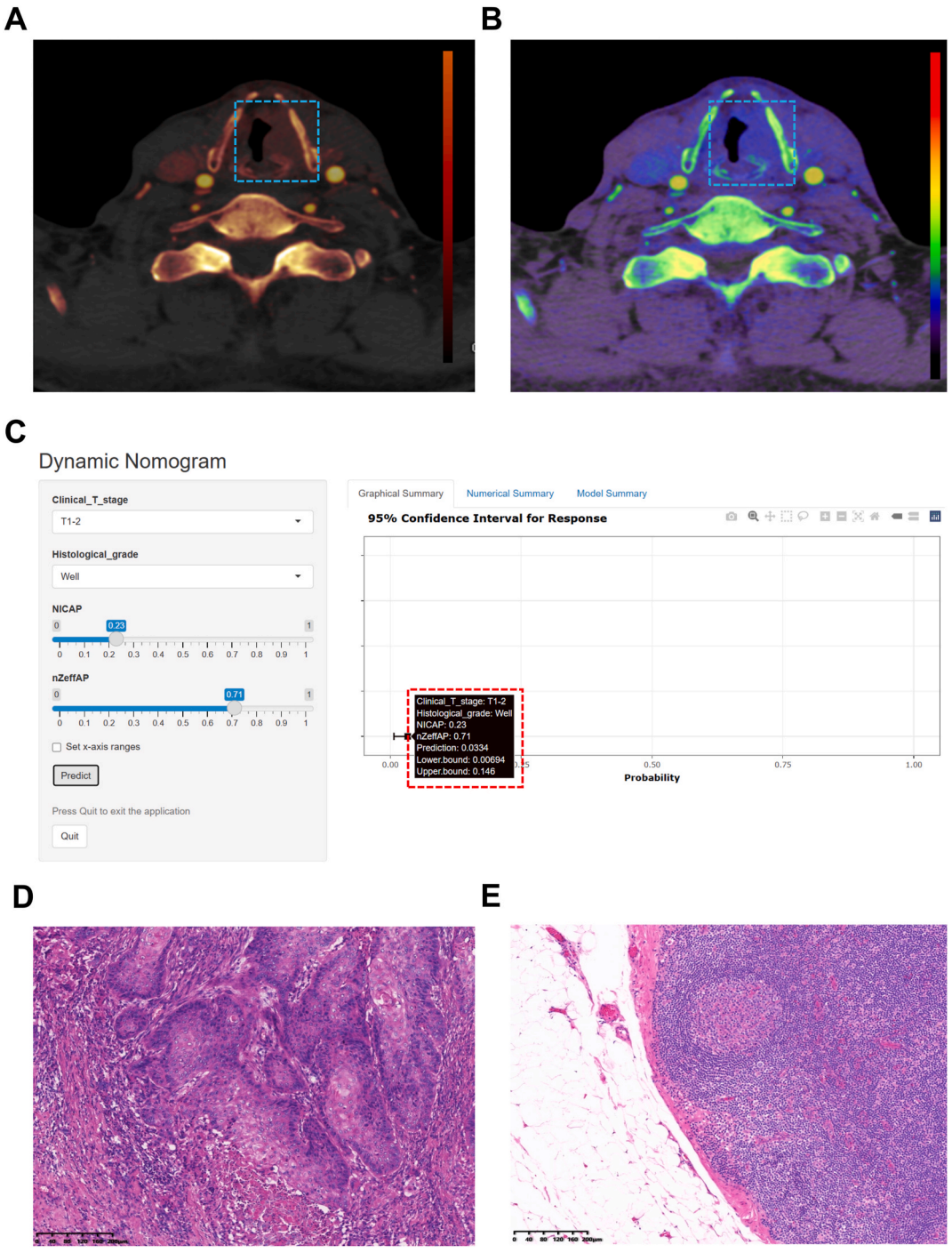

Fig. 6. A 67-year-old male with hoarseness for 6 months. Pathology results revealed well-differentiated LSCC with no metastasis in the cervical lymph nodes. **A:** Iodine map showing NIC of 0.23 in the arterial phase; **B:** Effective atomic number diagram showing nZ_{eff} of 0.71 in the arterial phase; **C:** The free browser-based model provides a corresponding probability of LNM (+) pathology of 3.3 %; **D, E:** Pathological pictures (× 100) proved LSCC **(D)** and no metastatic lymph nodes **(E)**. LNM, lymph node metastasis; LSCC, laryngeal squamous cell carcinoma; NIC, normalized iodine concentration; nZ_{eff}, normalized effective atomic number.

is in agreement with the results of previous retrospective studies [35,39]. Clinical decisions regarding neck treatment are usually based on a comprehensive analysis of T stage, tumour location, and CT reports [40]. However, although patients with supraglottic tumours may be more prone to LNM because of the extensive submucosal lymphatic plexus, we did not observe a significant association between tumour location and LNM, possibly due to the small number of patients with supraglottic disease in our study [41]. Generally,

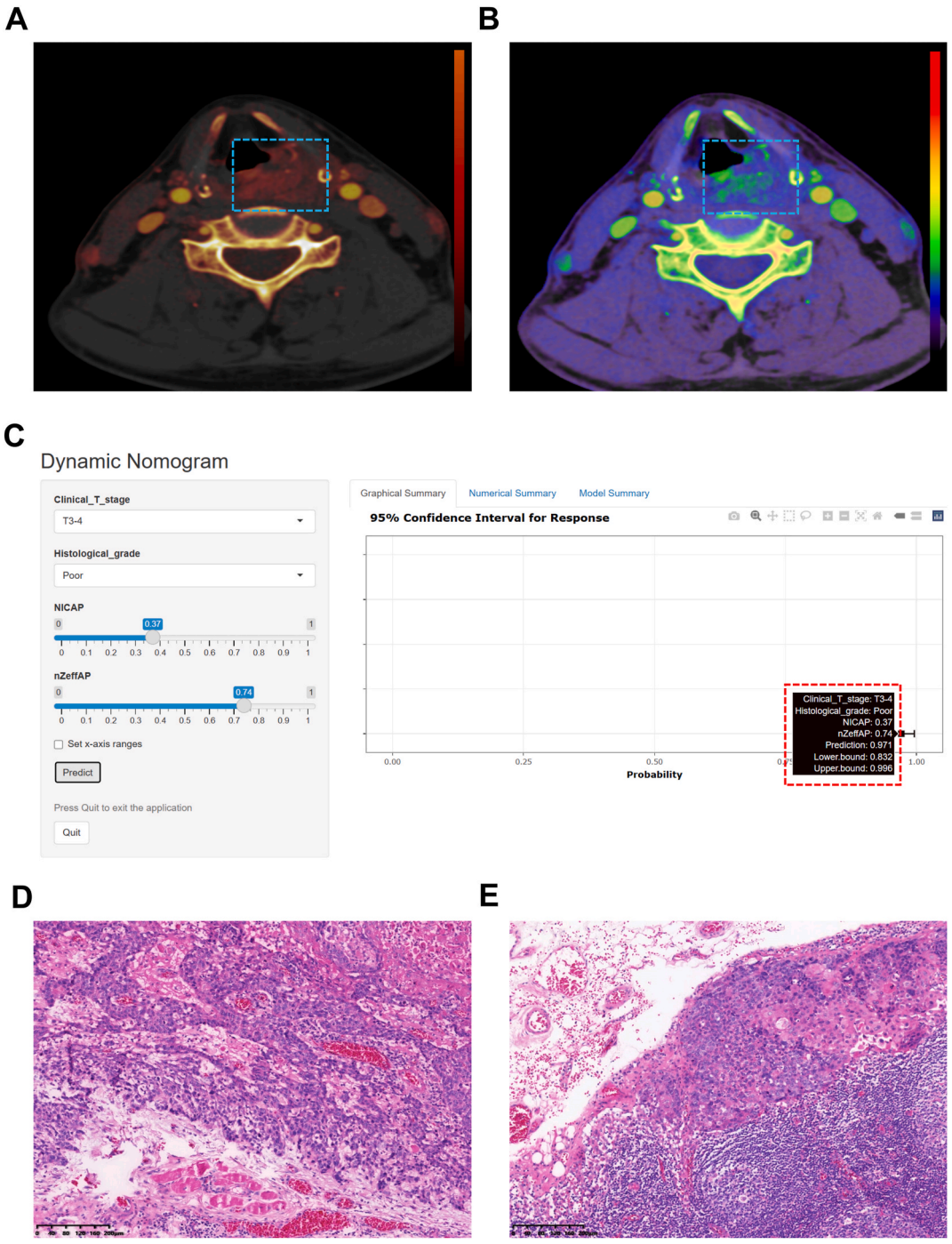

Fig. 7. A 73-year-old male with recurrent hoarseness for 4 years and dyspnea for 2 months. Pathology results revealed poorly differentiated LSCC with metastasis in the cervical lymph nodes. **A:** Iodine map showing NIC of 0.37 in the arterial phase; **B:** Effective atomic number diagram showing nZ_{eff} of 0.74 in the arterial phase; **C:** The free browser-based model provides a corresponding probability of LNM (+) of 97.1 %; **D, E:** Pathological pictures (× 100) proved LSCC **(D)** and metastatic lymph nodes in the level IV region **(E)**. LNM, lymph node metastasis; LSCC, laryngeal squamous cell carcinoma; NIC, normalized iodine concentration; nZ_{eff}, normalized effective atomic number.

poorly differentiated tumours are considered highly malignant. Consistent with previous studies, we found that patients with poorly differentiated tumours had a higher incidence of LNM [21,42]. Furthermore, multivariate analysis revealed that clinical T stage and histological grade were independent risk factors for LNM in patients with LSCC. However, based on the clinical model, the AUCs for these two variables were only 0.788 and 0.764 in the training and validation cohorts, respectively. These findings suggest that

assessing the LN status based solely on clinical characteristics is likely to be unreliable, and more objective quantitative indicators must be identified to compensate for these deficiencies.

Following tumour cell infiltration of LNs, metastasis is a developmental process driven by pathological tumour angiogenesis and a continuous blood supply [43]. Previous studies have shown a significant positive correlation between IC and microvascular disease, suggesting that IC can be used as an indirect quantitative indicator of tumour blood perfusion [44]. The NIC is the corrected IC value that reduces individual circulatory differences [32]. Our results showed that NIC values of primary tumours were significantly higher in patients who were LNM (+) than in those who were LNM (−), which is similar to findings from Geng's study [19]. As the tumour grows, neovascularization increases significantly, whereas the basement membrane remains underdeveloped, resulting in vascular endothelial dysfunction. This, in turn, leads to increased iodine accumulation within the tumour [16]. Furthermore, patients with LSCC have a higher NIC in the arterial phase than in the venous phase. One possible reason for this is that the ROI was initially delineated in the most enhanced region in the arterial-phase image, followed by the same region in the venous-phase image. This is because most of the dynamic enhancement curves of head and neck tumours are of the rapidly rising plateau type, reaching a peak within 14–42 s [45]. Therefore, NICAP can reflect the characteristics of LSCC more accurately than NICVP.

The slope of the curve, which reflects the magnitude of the mass absorption coefficient with energy for various lesions and tissues, can be used to quantitatively evaluate the difference between energy spectrum curves [32]. In our study, λ_{HU} was not confirmed as an independent predictor for assessing LNM in patients with LSCC; however, λ_{HU} values of patients in the LNM (+) group still tended to be higher than those in the LNM (−) group. This difference can be explained by the effects of tumour cell migration on cell proliferation. Anomalous proliferation of tumour cells is one of the causes of tumour heterogeneity [46]. Thus, various tumour components or tissues result in distinct energy spectrum curves. Another important parameter for distinguishing the different components is nZ_{eff}. When the tumour density is higher, nZ_{eff} values increase. We found that higher nZ_{eff} values were more likely in the LNM (+) group, which may be due to the greater volumes of nuclei and cytoplasm, and higher macromolecular protein content in tumour tissues undergoing metastasis, subsequently leading to an increase in cell density. Our findings are further supported by a recent study showing that the apparent diffusion coefficient for quantifying the diffusion of water molecules in tissues was significantly lower in patients who were LNM (+) than in those who were LNM (−) ($P < 0.001$), and this value was negatively correlated with cell density within the tissue [47].

By constructing a nomogram, we were able to develop an easy-to-use, free, browser-based model for the objective assessment of the risk of pathological LNM, thereby providing a reliable reference tool for clinicians deciding on different interventions. For patients without clinical evidence of LNM, recommendations have included elective neck dissection, radiation treatment, and 'wait-and-see', with therapeutic dissection if metastasis develops during follow-up [48]. Neck dissection is recommended if the risk of occult neck metastasis is $>$ 15–20 % [49]. However, if the risk of occult LNM is low, neck overtreatment should be avoided to reduce complications, such as recurrent laryngeal nerve palsy, haematoma, and chyle leakage [50]. The prediction model integrated DECT quantitative parameters, T stage, and histological grade and showed a more accurate estimation of pathological LN status than the clinical model. This suggests that the DECT parameters can generate more predictive information than the clinical features. Nevertheless, in real-world clinical settings, the final treatment decision should be made only after a comprehensive evaluation of the model results, as well as preoperative, intraoperative, and postoperative evaluations of patients with LSCC.

This study had several limitations. First, this was a single-centre retrospective study, which should be validated with larger cohorts from multiple centres and prospective studies. Second, the ROI was drawn manually in this study, which was time- and labour-intensive and increased the potential risk of selection bias. This could be resolved using semi-automatic/automatic analysis based on whole-tumour ROI in the future. Third, owing to the limited sample size, we did not perform subgroup analyses according to the different subsites or stages of LSCC. Previous studies have reported that LNM is likely to occur in supraglottic carcinoma but is rarely encountered in early tumours [51]. Thus, a larger sample size is required for the subgroup analyses. Finally, images were acquired using a DECT scanner from Siemens Medical Solutions, and further research clarifying the influence of different DECT platforms is needed.

5. Conclusions

Our research has significant implications for treatment guidelines as the approach towards treating patients with LSCC remains controversial. The early detection and accurate assessment of cervical LNM are crucial for improving patient prognosis. DECT parameters (NICAP and $nZ_{eff}AP$) were used as imaging biomarkers to evaluate cervical LNM in patients with LSCC. By constructing a nomogram combining DECT parameters and clinical features (clinical T stage and histological grade), we developed an online prediction tool to assess LNM probability quickly and objectively. This can help clinicians select appropriate clinical treatment options and reduce neck overtreatment in these patients.

Funding statement

This work was supported by the Natural Science Foundation of Zhejiang Province (Grant No. LY23H180003 to Jianfei Tu), Medical and Health General Project of Zhejiang Province (Grant No. 2024KY568 to Weiyue Chen, and No. 2023KY425 to Guihan Lin).

Data availability statement

Data will be made available on request.

CRediT authorship contribution statement

Jianfei Tu: Writing – review & editing, Writing – original draft, Funding acquisition, Formal analysis, Conceptualization, Resources. **Guihan Lin:** Writing – original draft, Project administration, Funding acquisition, Formal analysis, Conceptualization, Data curation, Writing – review & editing. **Weiyue Chen:** Writing – review & editing, Project administration, Funding acquisition, Formal analysis, Methodology, Writing – original draft. **Feng Cheng:** Data curation, Supervision. **Haifeng Ying:** Methodology, Formal analysis. **Chunli Kong:** Investigation. **Dengke Zhang:** Supervision, Validation. **Yi Zhong:** Software. **Yongjun Ye:** Methodology, Investigation. **Minjiang Chen:** Writing – review & editing, Visualization, Validation, Supervision, Resources. **Chenying Lu:** Conceptualization, Software. **Xiaomin Yue:** Investigation, Resources. **Wei Yang:** Writing – review & editing, Conceptualization, Investigation, Methodology, Resources.

Declaration of competing interest

The authors declare that they have no known competing financial interests or personal relationships that could have appeared to influence the work reported in this paper.

Appendix A. Supplementary data

Supplementary data to this article can be found online at https://doi.org/10.1016/j.heliyon.2024.e35528.

References

[1] D.E. Johnson, B. Burtness, C.R. Leemans, V.W.Y. Lui, J.E. Bauman, J.R. Grandis, Head and neck squamous cell carcinoma, Nat. Rev. Dis. Prim. 6 (1) (2020) 92.
[2] H. Sung, J. Ferlay, R.L. Siegel, et al., Global cancer statistics 2020: GLOBOCAN estimates of incidence and mortality worldwide for 36 cancers in 185 countries, CA: a cancer journal for clinicians 71 (3) (2021) 209–249.
[3] J.D. Cramer, B. Burtness, Q.T. Le, R.L. Ferris, The changing therapeutic landscape of head and neck cancer, Nat. Rev. Clin. Oncol. 16 (11) (2019) 669–683.
[4] X. Wang, L. Tian, Y. Li, et al., RBM15 facilitates laryngeal squamous cell carcinoma progression by regulating TMBIM6 stability through IGF2BP3 dependent, Journal of experimental & clinical cancer research : CR 40 (1) (2021) 80.
[5] A. Ferlito, A. Rinaldo, C.E. Silver, et al., Neck dissection for laryngeal cancer, J. Am. Coll. Surg. 207 (4) (2008) 587–593.
[6] A.A. Forastiere, N. Ismaila, G.T. Wolf, Use of larynx-preservation strategies in the treatment of laryngeal cancer: American society of clinical Oncology clinical practice guideline update summary, Journal of oncology practice 14 (2) (2018) 123–128.
[7] B.J. Baird, C.K. Sung, B.M. Beadle, V. Divi, Treatment of early-stage laryngeal cancer: a comparison of treatment options, Oral Oncol. 87 (2018) 8–16.
[8] K. Bhattacharya, A. Mahajan, R. Vaish, S. Rane, S. Shukla, A.K. D'Cruz, Imaging of neck nodes in head and neck cancers - a comprehensive update, Clin. Oncol. 35 (7) (2023) 429–445.
[9] H.J. Lee, J. Kim, H.Y. Woo, W.J. Kang, J.H. Lee, Y.W. Koh, 18F-FDG PET-CT as a supplement to CT/MRI for detection of nodal metastasis in hypopharyngeal SCC with palpably negative neck, Laryngoscope 125 (7) (2015) 1607–1612.
[10] M.C. Ketterer, L.A. Lemus Moraga, U. Beitinger, J. Pfeiffer, A. Knopf, C. Becker, Surgical nodal management in hypopharyngeal and laryngeal cancer, Eur. Arch. Oto-Rhino-Laryngol. : official journal of the European Federation of Oto-Rhino-Laryngological Societies (EUFOS) : affiliated with the German Society for Oto-Rhino-Laryngology - Head and Neck Surgery 277 (5) (2020) 1481–1489.
[11] J. Sun, B. Li, C.J. Li, et al., Computed tomography versus magnetic resonance imaging for diagnosing cervical lymph node metastasis of head and neck cancer: a systematic review and meta-analysis, OncoTargets Ther. 8 (2015) 1291–1313.
[12] T.R. Johnson, B. Krauss, M. Sedlmair, et al., Material differentiation by dual energy CT: initial experience, Eur. Radiol. 17 (6) (2007) 1510–1517.
[13] C.H. McCollough, K. Boedeker, D. Cody, et al., Principles and applications of multienergy CT: report of AAPM task group 291, Medical physics 47 (7) (2020) e881–e912.
[14] R. Forghani, An update on advanced dual-energy CT for head and neck cancer imaging, Expet Rev. Anticancer Ther. 19 (7) (2019) 633–644.
[15] Y.H. Luo, X.L. Mei, Q.R. Liu, et al., Diagnosing cervical lymph node metastasis in oral squamous cell carcinoma based on third-generation dual-source, dual-energy computed tomography, Eur. Radiol. 33 (1) (2023) 162–171.
[16] Y. Zou, S. Sun, Q. Liu, et al., A new prediction model for lateral cervical lymph node metastasis in patients with papillary thyroid carcinoma: based on dual-energy CT, Eur. J. Radiol. 145 (2021) 110060.
[17] K. Terada, H. Kawashima, N. Yoneda, et al., Predicting axillary lymph node metastasis in breast cancer using the similarity of quantitative dual-energy CT parameters between the primary lesion and axillary lymph node, Jpn. J. Radiol. 40 (12) (2022) 1272–1281.
[18] L. Qiu, J. Hu, Z. Weng, S. Liu, G. Jiang, X. Cai, A prospective study of dual-energy computed tomography for differentiating metastatic and non-metastatic lymph nodes of colorectal cancer, Quant. Imag. Med. Surg. 11 (8) (2021) 3448–3459.
[19] D. Geng, X. Chen, X.G. Zhao, et al., Laryngeal and hypopharyngeal squamous cell carcinoma: association between quantitative parameters derived from dual-energy CT and histopathological prognostic factors, Acta radiologica (Stockholm, Sweden 2022 (1987) 2841851221095237.
[20] J.J. Caudell, M.L. Gillison, E. Maghami, et al., NCCN Guidelines® insights: head and neck cancers, version 1.2022, J. Natl. Compr. Cancer Netw. : J. Natl. Compr. Cancer Netw. 20 (3) (2022) 224–234.
[21] L. Song, Y. Heng, C.Y. Hsueh, et al., A predictive nomogram for lymph node metastasis in supraglottic laryngeal squamous cell carcinoma, Front. Oncol. 12 (2022) 786207.
[22] P. Goldstraw, K. Chansky, J. Crowley, et al., The IASLC lung cancer staging Project: proposals for revision of the TNM stage groupings in the forthcoming (eighth) edition of the TNM classification for lung cancer, J. Thorac. Oncol. : official publication of the International Association for the Study of Lung Cancer 11 (1) (2016) 39–51.
[23] A.A. Forastiere, N. Ismaila, J.S. Lewin, et al., Use of larynx-preservation strategies in the treatment of laryngeal cancer: American society of clinical Oncology clinical practice guideline update, J. Clin. Oncol. : official journal of the American Society of Clinical Oncology 36 (11) (2018) 1143–1169.
[24] C. Li, L. Chen, J. Wang, et al., Expression and clinical significance of cathepsin B and stefin A in laryngeal cancer, Oncol. Rep. 26 (4) (2011) 869–875.
[25] S. Petrarolha, R. Dedivitis, L. Matos, D. Ramos, M. Kulcsar, Lymph node density as a predictive factor for worse outcomes in laryngeal cancer, Eur. Arch. Oto-Rhino-Laryngol. : official journal of the European Federation of Oto-Rhino-Laryngological Societies (EUFOS) : affiliated with the German Society for Oto-Rhino-Laryngology - Head and Neck Surgery 277 (3) (2020) 833–840.
[26] S.X. Wang, W.J. Ning, X.W. Zhang, P.Z. Tang, Z.J. Li, W.S. Liu, Predictors of occult lymph node metastasis and prognosis in patients with cN0 T1-T2 supraglottic laryngeal carcinoma: a retrospective study, ORL J. Oto-Rhino-Laryngol. its Relat. Specialties 81 (5–6) (2019) 317–326.

[27] H.H. Coskun, J.E. Medina, K.T. Robbins, et al., Current philosophy in the surgical management of neck metastases for head and neck squamous cell carcinoma, Head Neck 37 (6) (2015) 915–926.
[28] L.Y. Chen, W.B. Weng, W. Wang, J.F. Chen, Analyses of high-risk factors for cervical lymph node metastasis in laryngeal squamous cell carcinoma and establishment of nomogram prediction model, Ear Nose Throat J. 100 (5_suppl) (2021), 657s-62s.
[29] J. Chen, F. Zhang, M. Hua, X. Song, S. Liu, Z. Dong, Prognostic value of lymphatic vessel density in oral squamous cell carcinoma, Life Sci. 265 (2021) 118746.
[30] G.B. Flach, E. Bloemena, A. van Schie, et al., Sentinel node identification in laryngeal cancer: feasible in primary cancer with previously untreated neck, Oral Oncol. 49 (2) (2013) 165–168.
[31] H. Shen, Y. Huang, X. Yuan, et al., Using quantitative parameters derived from pretreatment dual-energy computed tomography to predict histopathologic features in head and neck squamous cell carcinoma, Quant. Imag. Med. Surg. 12 (2) (2022) 1243–1256.
[32] P. Wang, Z. Tang, Z. Xiao, et al., Dual-energy CT in predicting Ki-67 expression in laryngeal squamous cell carcinoma, Eur. J. Radiol. 140 (2021) 109774.
[33] F. Li, F. Huang, C. Liu, et al., Parameters of dual-energy CT for the differential diagnosis of thyroid nodules and the indirect prediction of lymph node metastasis in thyroid carcinoma: a retrospective diagnostic study, Gland Surg. 11 (5) (2022) 913–926.
[34] X. Yang, H. Hu, F. Zhang, et al., Preoperative prediction of the aggressiveness of oral tongue squamous cell carcinoma with quantitative parameters from dual-energy computed tomography, Front. Oncol. 12 (2022) 904471.
[35] Ö. Bayır, G. Toptaş, G. Saylam, et al., Occult lymph node metastasis in patients with laryngeal cancer and relevant predicting factors: a single-center experience, Tumori 108 (5) (2022) 439–449.
[36] A.C. Birkeland, A.J. Rosko, M.R. Issa, et al., Occult nodal disease prevalence and distribution in recurrent laryngeal cancer requiring salvage laryngectomy, Otolaryngology–head and neck surgery : official journal of American Academy of Otolaryngology-Head and Neck Surgery 154 (3) (2016) 473–479.
[37] Q. Zhang, Y. Xiong, L. Lin, K. Yuan, Analysis of related factors of surgical treatment effect on 215 patients with laryngeal cancer, Exp. Ther. Med. 15 (3) (2018) 2786–2791.
[38] D.D. Sharbel, M. Abkemeier, M.W. Groves, W.G. Albergotti, J.K. Byrd, C. Reyes-Gelves, Occult metastasis in laryngeal squamous cell carcinoma: a systematic review and meta-analysis, Ann. Otol. Rhinol. Laryngol. 130 (1) (2021) 67–77.
[39] X. Zhao, W. Li, J. Zhang, et al., Radiomics analysis of CT imaging improves preoperative prediction of cervical lymph node metastasis in laryngeal squamous cell carcinoma, Eur. Radiol. 33 (2) (2023) 1121–1131.
[40] A. Ferlito, A. Rinaldo, C.E. Silver, et al., Neck dissection: then and now, Auris Nasus Larynx 33 (4) (2006) 365–374.
[41] T. Yılmaz, N. Süslü, G. Atay, R. Günaydın, M.D. Bajin, S. Özer, The effect of midline crossing of lateral supraglottic cancer on contralateral cervical lymph node metastasis, Acta Otolaryngol. 135 (5) (2015) 484–488.
[42] A. Al-Kaabi, R.S. van der Post, J. Huising, C. Rosman, I.D. Nagtegaal, P.D. Siersema, Predicting lymph node metastases with endoscopic resection in cT2N0M0 oesophageal cancer: a systematic review and meta-analysis, United European gastroenterology journal 8 (1) (2020) 35–43.
[43] S. Rizzo, D. Radice, M. Femia, et al., Metastatic and non-metastatic lymph nodes: quantification and different distribution of iodine uptake assessed by dual-energy CT, Eur. Radiol. 28 (2) (2018) 760–769.
[44] J. Marcon, A. Graser, D. Horst, et al., Papillary vs clear cell renal cell carcinoma. Differentiation and grading by iodine concentration using DECT-correlation with microvascular density, Eur. Radiol. 30 (1) (2020) 1–10.
[45] J.E. Park, J.H. Lee, K.H. Ryu, et al., Improved diagnostic accuracy using arterial phase CT for lateral cervical lymph node metastasis from papillary thyroid cancer, AJNR American journal of neuroradiology 38 (4) (2017) 782–788.
[46] H. Liang, A. Li, Y. Li, et al., A retrospective study of dual-energy CT for clinical detecting of metastatic cervical lymph nodes in laryngeal and hypopharyngeal squamous cell carcinoma, Acta Otolaryngol. 135 (7) (2015) 722–728.
[47] J. Zhao, X. Li, M. Wang, F. Liu, J. Wang, Diagnostic value of MRI combined with CXCR4 expression level in lymph node metastasis head and neck squamous cell carcinoma, Comput. Math. Methods Med. 2022 (2022) 4073918.
[48] J.P. Rodrigo, J.P. Shah, C.E. Silver, et al., Management of the clinically negative neck in early-stage head and neck cancers after transoral resection, Head Neck 33 (8) (2011) 1210–1219.
[49] A. Sanabria, J.P. Shah, J.E. Medina, et al., Incidence of occult lymph node metastasis in primary larynx squamous cell carcinoma, by subsite, T classification and neck level: a systematic review, Cancers 12 (4) (2020).
[50] A.R. Shaha, Complications of neck dissection for thyroid cancer, Ann. Surg Oncol. 15 (2) (2008) 397–399.
[51] Y. Choi, M. Bin-Manie, J.L. Roh, et al., Metastatic lymph node burden predictive of survival in patients undergoing primary surgery for laryngeal and hypopharyngeal cancer, J. Cancer Res. Clin. Oncol. 145 (10) (2019) 2565–2572.